Vrije Universiteit Brussel

Assessing effects of ultra-high-pressure liquid chromatography instrument configuration on dispersion, system pressure, and retention

Zhou, Zhuoheng; De Pra, Mauro; Steiner, Frank; Desmet, Gert; Eeltink, Sebastiaan

Published in:
Journal of Chromatography A

DOI:
10.1016/j.chroma.2020.461660

Publication date:
2020

License:
CC BY-NC-ND

Document Version:
Accepted author manuscript

Link to publication

Citation for published version (APA):
Zhou, Z., De Pra, M., Steiner, F., Desmet, G., & Eeltink, S. (2020). Assessing effects of ultra-high-pressure liquid chromatography instrument configuration on dispersion, system pressure, and retention. *Journal of Chromatography A*, *1634*, [461660]. https://doi.org/10.1016/j.chroma.2020.461660

Copyright
No part of this publication may be reproduced or transmitted in any form, without the prior written permission of the author(s) or other rights holders to whom publication rights have been transferred, unless permitted by a license attached to the publication (a Creative Commons license or other), or unless exceptions to copyright law apply.

Take down policy
If you believe that this document infringes your copyright or other rights, please contact openaccess@vub.be, with details of the nature of the infringement. We will investigate the claim and if justified, we will take the appropriate steps.

Download date: 11. Apr. 2024

Assessing effects of ultra-high-pressure liquid chromatography instrument configuration on dispersion, system pressure, and retention

Zhuoheng Zhou[1], Mauro De Pra[2], Frank Steiner[2], Gert Desmet[1], Sebastiaan Eeltink[1,*]

[1]Vrije Universiteit Brussel (VUB), Department of Chemical Engineering, Brussels, Belgium

[2]Thermo Fisher Scientific, Germering, Germany

(*) corresponding author

Pleinlaan 2, B-1050, Brussels, Belgium

Tel.: +32 (0)2 629 3324, Fax: +32 (0)2 629 3248, E-mail: seeltink@vub.be

Abstract

This study involves the systematic assessment of the effects of system configuration on dispersion, pressure, and retention characteristics while operating a 1500 bar UHPLC system with 2.1 mm i.d. × 100 mm long columns packed with 1.5 µm core-shell particles in isocratic and gradient mode. Altering the system configuration by changing the i.d. of connection tubing and flow cells affects the elution time, dispersion characteristics, and the kinetic performance limits of the system. The gain in separation efficiency when decreasing tubing i.d. from 100 to 75 µm was found to contribute more to the decrease in separation impedance and the position of the kinetic performance curve than the loss in available column pressure induced by the narrower tubing. When applying steep gradients, characterized by gradient-to-column dead-time ratio < 7, optimizing instrument configuration leads to either a significant time gain factor of 3.9 without compromising peak capacity, or a gain in peak capacity with a gain factor of 1.3 while maintaining the analysis time constant. Due to the reduced fluidic volume of connection tubing of smaller i.d., a decrease in residence time is obtained. At the same time, an increase in *k* was observed due to a pressure-induced retention effect, and this effect is significant for late-eluting analytes.

Keywords: ultra-high-pressure LC; extra-column band broadening; method development

1. Introduction

Advancements in stationary-phase developments and LC system design have paved the way for ultra-high-pressure liquid chromatography (UHPLC) with leaps in both separation efficiency and analysis throughput [1]. Pivotal proof-of-concept research in the field of UHPLC has been conducted by the Jorgenson research group [2,3]. Back in 1997 this group reported already on high-efficiency separations using 1.5 μm nonporous silica C_{18} particles packed in small i.d. columns to minimize frictional heating [2]. These concepts have been adopted and ultimately led to the development of the first commercially available UHPLC system [4]. The current state-of-art UHPLC instrument allows to operate 2.1 mm i.d. narrow-bore column packed with sub-2-μm particles at operating pressures up to 1500 bar [5].

The increase in separation efficiency by using smaller particles and the reduction in column inner diameter have resulted in decreasingly smaller peak volumes, which necessitates the according reduction of extra-column dispersion contributions. A widely accepted criterion for the loss in resolution caused by external dispersion ($\sigma^2_{v,ext}$) is 5% [6], which corresponds to ≅ 10% in decrease in plate number. When considering the total peak variance ($\sigma^2_{v,tol}$) as the sum of dispersion inside the column ($\sigma^2_{v,col}$) and $\sigma^2_{v,ext}$, the observed system efficiency (N_{obs}) is given by [7]:

$$N_{obs} = N_{col} \cdot \frac{\sigma^2_{v,col}}{\sigma^2_{v,col}+\sigma^2_{v,ext}} \quad (1)$$

In isocratic separation mode, $\sigma^2_{v,col}$ can be written as [8,9]:

$$\sigma^2_{v,col} = \frac{V_0^2}{N_{col}} \cdot (1+k)^2 \quad (2)$$

where V_0 is the column dead volume and k is the analyte retention factor. Eqs. 1 and 2 illustrate that the observed plate numbers (N_{obs}) of early-eluting analytes are sensitive to extra-column dispersion. Furthermore, given high efficiency (higher N_{col}) and small i.d. (yielding lower V_0)

are the features of state-of-the-art UHPLC column, extra-column dispersion exhibits a critical role in observed system efficiency (N_{obs}) [10,11].

$\sigma^2_{v,ext}$ is often assumed as the sum of the dispersion induced upon injection ($\sigma^2_{v,inj}$), pre-column tubing ($\sigma^2_{v,pre-tub}$), post-column tubing ($\sigma^2_{v,post-tub}$), and detection ($\sigma^2_{v,det}$):

$$\sigma^2_{v,ext} = \sigma^2_{v,inj} + \sigma^2_{v,pre-tub} + \sigma^2_{v,post-tub} + \sigma^2_{v,det} \quad (3)$$

Note that also column hardware, *i.e.*, bore diameter and frit design contribute to the total peak variance observed. Nowadays, most of the UHPLC manufacturers provide commercial high-pressure compatible injectors, connecting tubing with minimized dispersion volume, and also flow-cell design has been reconsidered to maximize detection sensitivity while minimizing the dispersion contribution [1]. The most practical approach to minimize extra-column dispersion is to reduce the i.d. of the extra-column flow path. However, the gain is obtained at the expense of a significant pressure drop induced by the system. For instance, by decreasing the tubing i.d. from 100 μm to 75 μm, the pressure drop on tubing alone will be around three times greater, and 16 times greater when going further down to 50 μm, as pressure is inversely proportional to the fourth power of inner diameter. As pointed out by Giddings [12], and Knox and Saleem [13], the attainable maximum theoretical plate count and analysis time are affected by the available pressure drop across the column. The introduction of extra system pressure by decreasing external fluidic volumes inevitably decreases the available column pressure when the maximum operating pressure is limited.

Different modeling and experimental approaches has be adopted to investigate the dispersions on individual flow-path component [7,8,10], however, few studies has focused on how do these dispersions affect system performance collectively, and little guidelines has been provided for practical UHPLC users when facing various choices of tubing and flow cells. In the present study, the instrument configuration of a UHPLC system with 1500 bar pressure

capability was systematically altered and effects of system configuration on the separation performance were assessed in both isocratic and gradient LC mode. Different visualization approaches have been adopted to discuss the effects of system configuration on chromatographic dispersion and combined effects on dispersion and available column pressure affecting kinetic performance limits (KPLs). In addition, the effect of tubing i.d. influencing elution time and column inlet pressure on retention factor have been explored.

2. Experimental

2.1. Chemicals and reagents

Uracil (99%), phenol (99%), acetophenone (99%), butyrophenone (99%), valerophenone (99%), hexanophenone (99%), heptanophenone (98%), octanophenone (99%), and benzanthracene (99%) were purchased from Sigma-Aldrich (Bornem, Belgium). Acetonitrile (ACN, HPLC grade) was obtained from Biosolve (Valkenswaard, The Netherlands). Ultra-pure water (18.2 MΩ·cm) was generated by a Milli-Q water purification system (Millipore, Molsheim, France). Uracil (t_0 marker), acetophenone, butyrophenone, valerophenone, hexanophenone, heptanophenone, octanophenone, and benzanthracene were dissolved separately in 70:30% (v/v) ACN:H_2O at 1 g/L as stock solutions. The sample was prepared by mixing and diluting aforementioned solutions in 70:30% (v/v) ACN:H_2O yielding 5 µL/L for acetophenone, 10 mg/L for uracil, 10 µL/L for phenol and butyrophenone, 20 µL/L for valerophenone, hexanophenone, heptanophenone, 20 mg/L for benzanthracene, and 30 µL/L for octanophenone.

2.2. Instrumentation and LC conditions

Separations were performed on a Vanquish Horizon UHPLC system (Thermo Fisher Scientific, Germering, Germany). The system consists of a binary parallel dual-piston ultra-high-pressure pump, thermostatted autosampler with a split-loop injector, thermostatted column compartment and a variable-wavelength UV detector (VWD). Chromeleon software (7.2 version) was used for system operation and data acquisition. Experiments were performed applying an injection volume of 0.5 μL, operating the column compartment in still-air mode at 35°C, and applying a UV wavelength at 210 nm with 50 Hz acquisition frequency (0 sec response time). Accucore Vanquish columns (2.1 mm i.d. × 100 mm length) packed with 1.5 μm core-shell C_{18} particles were obtained from Thermo Fisher Scientific (Runcorn, UK). Two different types of tubing were applied to connect the column to the injection valve and flow cell, *i.e.*, 75 μm i.d. × 350 mm length silica nanoViper and 100 μm i.d. × 350 mm length Viper made of MP35N alloy (Thermo Fisher Scientific). Flow cells with internal volumes of 2.5 μL (100 μm i.d.) and 45 nL (average 75 μm i.d.) were used, respectively. Isocratic separations were performed with a binary mobile phase of 70:30% (v/v) ACN:H_2O. Gradient separations were conducted applying 3 and 10 min linear aqueous ACN gradients and the gradient span was fixed from 30:70% (v/v) ACN:H_2O to 100 v% ACN.

3. Results and discussion

3.1. Performance characterization in isocratic mode

The system performance was assessed in isocratic mode operating columns close to the optimum van Deemter flow rate (F = 0.4 mL/min) for given analytes and mobile-phase composition applied, and applying different tubing and flow cell configurations as summarized in Table I. Extra-column variances ($\sigma^2_{v,ext}$) are also provided by fitting experiment data (N_{obs} vs k) into Eq.1 and Eq. 2 (V_0 was obtained by t_0 measurement, column efficiency was thus

determined to be 41452). Intrinsic peak variances $\sigma^2_{v,col}$ (column only) varied between 0.9 and 32 μL^2 (for *k* between 0.2 and 6.1) and corresponding asymmetry factors ranged between 1.4 and 1.08. Fig. 1A depicts an overlay of chromatograms recorded using configuration #3 and #6, respectively. Narrower peaks were observed for all the compounds tested in configuration #3 because the extra-column dispersion was reduced when using pre- and post-column tubing having an inner diameter of 75 µm compared to configuration #6 that used tubing having an inner diameter of 100 µm. In addition, changing to configurations with narrower tubing led to a bidirectional shift on elution time. On one hand, reduced external fluidic volumes caused by decreased tubing i.d. resulted in a decrease of total residence time (equal contribution for individual compounds, details are shown in SM1). On the other hand, the extra system pressure introduced by narrow tubing contributed to an increase in retention, in which late-eluting compounds were more affected (see also discussion in *'Section 3.3'*). Hence, the net result was a decrease in elution time for early-eluting compounds (Fig. 1B) and *vice versa* for the late-eluting compounds (Fig. 1C).

Fig 2. provides quantitative insights in the effects of the system configuration on separation efficiency, KPLs, and separation impedance (*E*), respectively. Fig. 2A visualizes the reduced plate height (*h*) as function of retention factor for the different system configurations. Decreasing the i.d. of the tubing led to a decrease in *h*, and the effect was more pronounced for early-eluting analytes, as their peak volumes were relatively small. Considering configuration #1 and #2, decreasing the UV flow cell volume clearly led to a significant decrease in *h*, yielding high separation efficiency for a broad range of analytes with a minimum reduced plate height of 1.74, implying a well-packed column and a relatively small eddy-diffusion (*A*-term) contribution to chromatographic dispersion, due to the core-shell nature of the particles and the narrow particle-size distribution.

No significant difference in configuration #4 and #5 was observed in cases where the solvent composition of the sample and mobile phase is matched, and no sample focusing effect at the column inlet was obtained. However, when dissolving the analytes in a weaker solvent than the mobile phase, *i.e.*, 50:50% (v/v) ACN:H_2O, a sample-focusing effect was observed leading to a slight decrease in *h*, which was more pronounced for early-eluting analytes (10.3% for k = 0.95 and 5.3% for k = 4.6). Given these conditions, the dispersion induced by the pre-column tubing i.d. is minimized and the configuration with smaller i.d. post-column tubing yielded the better results (see Fig. S1 in SM2). Alternatively, the performance optimizing injection sequence (POISe) can be applied to minimize precolumn dispersion [14], however, peak symmetry may be compromised [15].

Fig. 2B shows the KPLs obtained using configuration #1 (75 µm i.d. pre- and post-column tubing and 45 nL flow cell) and #6 (100 µm i.d. pre- and post-column tubing and 2.5 µL flow cell) when operating at a maximum system pressure of 1500 bar. This representation incorporates the effects of system configuration on both efficiency and system pressure, according to [16]:

$$N_{max} = \frac{\Delta P_{max}}{\eta} \cdot \frac{K_v}{u_0 \cdot H} \quad (4)$$

$$t_{0,max} = \frac{\Delta P_{max}}{\eta} \cdot \frac{K_v}{u_0^2} \quad (5)$$

where N_{max} and $t_{0,max}$ are the separation efficiency and column dead time obtained as the KPLs, ΔP_{max} is the maximum operating pressure, η is the viscosity of the mobile phase, K_v is the permeability taking into account the pressure drop across both the column and the system, u_0 is the mobile-phase velocity, and H is the observed plate height. Fig. 2B shows that the KPLs are affected by the instrument configuration for the early-eluting analytes (dotted trend lines). The gain in separation efficiency obtained when using configuration #1 contributed more to the position of the kinetic performance curve than the loss in available column pressure induced

when using narrower tubing. As the peak volumes of late-eluting analytes are significantly larger, the peak widths are less negatively affected by the instrument configuration. Also note that with increasing column length, the peak volumes increase (see the upper right corner of the kinetic plot in Fig. 2B), which leads to converging trend lines. Therefore, the effect of system configuration on the resulting performance limits become less pronounced in this part of the kinetic plot.

Fig. 2C shows an alternative representation to compare the system performance based on the separation impedance (*E*), taking into account both the column and extra-column contributions to dispersion and pressure, defined as [17]:

$$E = \frac{H^2}{K_v} = \frac{t_R \cdot \Delta P}{N^2 \cdot \eta \cdot (1+k)} \quad (6)$$

The major differentiator inducing a change in separation impedance was the flow cell design, in particular the i.d. of the optical path, which differentiates configuration #1 and #2 from the other configurations. This phenomenon has also been observed when comparing system performance between HPLC and UHPLC using same column [10]. Another contributor to performance is tubing i.d. When comparing configuration #3 (75 µm i.d. tubing) with that of #6 (100 µm i.d. tubing), it becomes apparent that configuration #3 yields a lower *E* value for early-eluting analytes, due to the better dispersion characteristics. As expected, configurations #4 and #5 yielded similar *E* values as peak variances on pre- and post-column tubing are additive at the mobile-phase condition applied (without sample focusing).

3.2. Gradient performance assessment

Extra-column dispersion effects induced by the system configuration on the resulting gradient performance were investigated while operating the column at a flow rate *F* = 0.4 mL/min and applying a conventional 10 min and a steep 3 min gradient, respectively, see Fig.

3 for typical chromatograms obtained with configuration #1. To visualize the gradient performance in analogy with the isocratic representation mode (Fig. 2A), the square of the four-sigma peak width (W) normalized by the observed retention time (t_R) was plotted as function of apparent retention factor k^*. Fig. 4A and Fig. 4B represent the results for the 10 min and 3 min gradient, respectively. A similar trend of instrument configuration effect on apparent efficiency is obtained as observed in isocratic mode, as the performance of early-eluting analytes ($k < 2$) is significantly deteriorated when using larger tubing and flow-cell i.d. Configuration #4 yielded a slightly better performance with respect to $(W/t_R)^2$ than #5 for early-eluting analytes and in the presence of a slight focusing effect. This indicates that the i.d. of post-columns fluidics is more critical to the overall performance than the i.d. of pre-column fluidics. The steeper the gradient, the smaller the peak volumes become [18]. As a result, these peaks are more affected by the extra-column dispersion. When applying the 10 min gradient and changing from configuration #1 to #6, leads to a 30% increase of $\Delta(W/t_R)^2$ for the last eluting analyte, whereas for the 3 min gradient the difference was 100%.

The kinetic plot method can be extended to assess the configuration effect on gradient performance limits while operating at a maximum system pressure. Due to the peak compression effect and the effect of the varying mobile-phase condition, the observed efficiency (N_{obs}) determined based on peak width and retention time does no longer represent the "true" separation performance [16,19]. Alternatively, using peak capacity (n_c) based on $4\sigma_t$ peak width determination in function of gradient time (t_G), is more practical to evaluate the system performance, according to [20–22]:

$$n_c = 1 + \frac{t_G}{4\sigma_t} \tag{7}$$

The resulting kinetic performance in gradient mode can be determined applying Eq. 8 and 9 (see SM3 for the detailed derivation):

$$n_{c,KPL} = 1 + \frac{1}{4} \cdot \sqrt{\frac{\Delta P_{max} \cdot K_V}{u_0 \cdot \eta \cdot H}} \cdot \frac{S \cdot \Delta\phi}{S \cdot \Delta\phi \cdot \frac{t_0}{t_G} + 1} \quad (8)$$

$$t_{R,KPL} = \frac{\Delta P_{max} \cdot K_V}{u_0^2 \cdot \eta} \cdot \left[1 + \frac{t_G}{t_0} \cdot \frac{1}{S \cdot \Delta\phi} \cdot ln\left(\frac{t_G}{t_0} \cdot \frac{k_0}{S \cdot \Delta\phi} + 1\right)\right] \quad (9)$$

where S is the slope of the linear relationship between ln k and organic solvent concentration, k_0 is the retention factor at the start of gradient, $\Delta\phi$ is the mobile-phase composition range.

The extrapolation of experimental gradient data to KPLs performed in this study is based on the assumption that analytes experience the same gradient profile, *i.e.*, same intrinsic gradient steepness b [18,19], independently of the column length applied:

$$b = S \cdot \Delta\phi \cdot \frac{t_0}{t_G} \quad (10)$$

Consequently, a constant gradient span $\Delta\phi$ and t_G/t_0 ratio needs to be applied for the construction of a fixed-length kinetic performance plot when varying the flow rate. The KPLs in gradient mode for a given system configuration can thus be obtained by extrapolating the experimentally determined peak capacity ($n_{c,exp}$), analysis time ($t_{R,exp}$) and pressure drop (ΔP_{exp}) measured on one specific column length. Fig. 5 shows the gradient KPLs for configuration #1 and #6 when operating at the maximum system pressure (1500 bar) and applying steep gradients ($t_G/t_0 = 7$ for a fixed $\Delta\phi = 0.7$). The analysis time on the y-axis represents the retention times for individual analytes. Considering the same configuration, the KPLs of the early- and late-eluting analytes lie close to each other, due to the fact that the peak widths of analytes experiencing a fixed solvent gradient are approximately similar [23,24].

Comparing the effect of the system configuration, the differences are however clear. The fact that configuration #1 largely outperforms system #6 implies that the gain in separation efficiency obtained when reducing the flow-cell volume and tubing i.d. is more contributing to the system performance limits than the loss in available column pressure induced by the

narrower tubing. Taking benzanthracene (apparent retention factor k^* = 7.2) for instance, this can either result in a significant gain in analysis time without losing performance, *i.e.*, the kinetic time gain factor for a fixed n_c = 220 is G_t = 22.2 min /5.7 min = 3.9. Alternatively, or a significant gain in peak capacity can be achieved for a fixed analysis time t_R= 4.5 min, *i.e.*, G_{nc} = 211 / 165 = 1.3.

3.3. Pressure-induced retention shifts

To ensure method transferability from HPLC to UHPLC system, good knowledge on chromatographic retention is required. When operating at optimum mobile phase velocity (F = 0.4 mL/min) elution time shifts were observed as demonstrated in Fig. 1. The net elution-time shifts result from the combination of a reduced residence time (as a higher linear velocity is generated in smaller i.d. tubing) and an increased retention time (as induced by extra system pressure when decreasing the i.d. of the tubing). While early-eluting analytes are dominated by the former effect (Fig.1B), the elution-time shift of late-eluted analytes are dominated by the latter (Fig. 1C). A similar trend was observed in gradient mode. A potential explanation for the increase in chromatographic retention can be linked to the increase in average column pressure induced by the smaller i.d. tubing, according to [25,26]:

$$\ln(\frac{k}{k'}) = -\frac{\Delta V}{RT} \cdot P + \ln(\frac{\beta}{\beta'}) \quad (11)$$

where k' and β' are the retention factor and the phase ratio taken as reference values at ambient condition. ΔV is the change in molecular volume when solutes transfer between mobile phase and stationary phase, R is the gas constant, and T is the temperature.

This phenomenon has been theoretically elaborated by Martin and Guiochon [27], and experimentally validated by several studies in the pressure range from 20 to 1000 bar [28–35]. A series of fatty acids (C10-C20) has been reported to exhibit increases in k from a range of

9%-24% for a pressure increase from 100 to 345 bar [34]. For small polar compounds, when average column pressure was increased from 20 to 500 bar, increase of 8-9% in retention factor at natural state and 11-15% when ionized were observed, respectively [29]. Both peptides and proteins have been found to be more sensitive to pressure change. ~2800% increase of ln (k) was observed for myoglobin (MW=17 kDa) for an increase in pressure from 100 to 1000 bar [35]. Given that typical external pressure drop in UHPLC system is in the order of 100 bar, by altering system configuration (varying i.d. of flow path) at high pressure range (> 500 bar), these differential changes in retention factor are far from negligible and can remain problematic on method transfer and validation for today's UHPLC users. To assess pressure-induced retention shifts, a series of chromatograms were recorded in isocratic mode by injecting the sample mixture and applying a fixed flow rate (F = 0.1 mL/min) while attaching restrictors after the UV detector. The low flow rate was selected to minimize frictional heating affecting chromatographic retention during the reference measurement. By adding restriction capillaries after the UV detector, the column inlet pressure increases while the pressure drop across the column remains the same, hence the frictional heat determined by Force × ΔP remains constant. This ensures the absence of frictional heating effect during experiments.

As shown in Fig. 6A, a linear relationship between the natural logarithm of retention factor and the column inlet pressure is observed, in agreement with Eq. 11. When increasing the column inlet pressure from 200 to almost 1200 bar, a notably change in retention factor is observed, *i.e.*, with a 7.2% increase for an early-eluting analyte (butyrophenone) while for benzanthracene the retention factor increased by 41%. Furthermore, it can be noted that pressure-induced retention effects are analyte dependent, as illustrated in Fig. 6B. Whereas a linear trend between molecular weight and pressure-induced retention change (in percentage) is observed for the homologue series of alkylphenones, benzanthracene (MW = 228.3 Da) yielding a significantly steeper slope in Fig. 6A and hence act as an outlier in Fig. 6B.

4. Conclusions

Extra-column dispersion and system-pressure effects induced by varying tubing and flow-cell configuration were systematically investigated in both isocratic and gradient separation modes. When using UHPLC technology allowing to operate 1.5 µm core-shell particle columns at pressures up to 1500 bar, system configuration significantly affects dispersion characteristics and resulting KPLs (considering dispersion and system pressure). Good UHPLC performance was generally obtained by applying flow-path components (tubing and flow cell) with narrow inner diameter tubing. Decreasing tubing i.d. from 100 to 75 µm led to a significant reduction in dispersion, while the loss in available column pressure did not compromise KPLs.

When sample-focusing conditions can be applied, *e.g.*, by increasing the water content in the sample, and/or using a highly retentive stationary phase, the i.d. of the post-column tubing contributes relatively more to dispersion than the pre-column tubing. Nevertheless, by plotting normalized peak variances against apparent retention factors, we demonstrated that the effect of instrumental dispersion in gradient separations is far from neglectable, especially when steeper gradient (characterized by smaller t_G/t_0 ratio) are applied. In this case, gradient KPLs (in terms of peak capacity and analysis time) are strongly affected by instrument configuration.

Altering system configuration can additionally render elution-time shifts, prompted by the change of residence time in the flow-path and pressure-induced retention effects. This is an important aspect that needs to be considered when comparing retention characteristics of different UHPLC systems with different fluidic configuration. Pressure-induced retention effects were quantitatively investigated by adding restrictors with different lengths behind the

UV detector. Theoretically predicted linear relationship between ln *k* and pressure was observed. The sensitivity of retention factor towards pressure change varies among analyte species and is likely related to the molecular weight, as demonstrated for a homologous series of alkylphenones.

5. Acknowledgements

Support of this work by an Excellence of Science grant (30897864) of the Research Foundation Flanders and the Fonds de la Recherche Scientifique (FWO-FRNS) is gratefully acknowledged.

6. References

[1] J. De Vos, K. Broeckhoven, S. Eeltink, J. De Vos, K. Broeckhoven, S. Eeltink, J. De Vos, K. Broeckhoven, S. Eeltink, Advances in ultrahigh-pressure liquid chromatography technology and system design, Anal. Chem. 88 (2016) 262–278.

[2] J.E. MacNair, K.C. Lewis, J.W. Jorgenson, Ultrahigh-pressure reversed-phase liquid chromatography in packed capillary columns, Anal. Chem. 69 (1997) 983–989.

[3] J.E. MacNair, K.D. Patel, J.W. Jorgenson, Ultrahigh-pressure reversed-phase capillary liquid chromatography: isocratic and gradient elution using columns packed with 1.0-μm particles, Anal. Chem. 71 (1999) 700–708.

[4] Q.A. Xu, Ultra-high performance liquid chromatography and its applications, John Wiley & Sons, Inc., Hoboken, NJ, USA, 2013.

[5] J. De Vos, M. De Pra, G. Desmet, R. Swart, T. Edge, F. Steiner, S. Eeltink, High-speed isocratic and gradient liquid-chromatography separations at 1500bar, J. Chromatogr. A. 1409 (2015) 138–145.

[6] J.P.C. Vissers, H.A. Claessens, C.A. Cramers, Microcolumn liquid chromatography:

instrumentation, detection and applications, J. Chromatogr. A. 779 (1997) 1–28.

[7] K. Vanderlinden, K. Broeckhoven, Y. Vanderheyden, G. Desmet, Effect of pre- and post-column band broadening on the performance of high-speed chromatography columns under isocratic and gradient conditions, J. Chromatogr. A. 1442 (2016) 73–82.

[8] F. Gritti, G. Guiochon, Accurate measurements of the true column efficiency and of the instrument band broadening contributions in the presence of a chromatographic column, J. Chromatogr. A. 1327 (2014) 49–56.

[9] F. Gritti, G. Guiochon, Accurate measurements of peak variances: Importance of this accuracy in the determination of the true corrected plate heights of chromatographic columns, J. Chromatogr. A. 1218 (2011) 4452–4461.

[10] K.J. Fountain, U.D. Neue, E.S. Grumbach, D.M. Diehl, Effects of extra-column band spreading, liquid chromatography system operating pressure, and column temperature on the performance of sub-2-μm porous particles, J. Chromatogr. A. 1216 (2009) 5979–5988.

[11] F. Gritti, G. Guiochon, On the extra-column band-broadening contributions of modern, very high pressure liquid chromatographs using 2.1mm I.D. columns packed with sub-2μm particles, J. Chromatogr. A. 1217 (2010) 7677–7689.

[12] J.C. Giddings, J.C. Gildings, J.C. Giddings, Comparison of Theoretical Limit of Separating Speed in Gas and Liquid Chromatography, Anal. Chem. 37 (1965) 60–63.

[13] J.H. Knox, M. Saleem, Kinetic conditions for optimum speed and resolution in column chromatography, J. Chromatogr. Sci. 7 (1969) 614–622.

[14] A.C. Sanchez, J.A. Anspach, T. Farkas, Performance optimizing injection sequence for minimizing injection band broadening contributions in high efficiency liquid chromatographic separations, J. Chromatogr. A. 1228 (2012) 338–348.

[15] M. Gilar, T.S. McDonald, G. Roman, J.S. Johnson, J.P. Murphy, J.W. Jorgenson,

Repetitive injection method: A tool for investigation of injection zone formation and its compression in microfluidic liquid chromatography, J. Chromatogr. A. 1381 (2015) 110–117.

[16] G. Desmet, D. Clicq, P. Gzil, Geometry-independent plate height representation methods for the direct comparison of the kinetic performance of LC supports with a different size or morphology, Anal. Chem. 77 (2005) 4058–4070.

[17] P.A. Bristow, J.H. Knox, Standardization of test conditions for high performance liquid chromatography columns, Chromatographia. 10 (1977) 279–289.

[18] L.R. Snyder, J.W. Dolan, High-performance gradient elution, John Wiley & Sons, Inc., Hoboken, NJ, USA, 2006.

[19] K. Broeckhoven, D. Cabooter, F. Lynen, P. Sandra, G. Desmet, The kinetic plot method applied to gradient chromatography: Theoretical framework and experimental validation, J. Chromatogr. A. 1217 (2010) 2787–2795.

[20] M.A. Stadalius, H.S. Gold, L.R. Snyder, Optimization model for the gradient elution separation of peptide mixtures by reversed-phase high-performance liquid chromatography. Verification of band width relationships for acetonitrile-water mobile phases, J. Chromatogr. A. 327 (1985) 27–45.

[21] X. Wang, D.R. Stoll, A.P. Schellinger, P.W. Carr, Peak capacity optimization of peptide separations in reversed-phase gradient elution chromatography: Fixed column format, Anal. Chem. 78 (2006) 3406–3416.

[22] M.A. Stadalius, H.S. Gold, L.R. Snyder, Optimization model for the gradient elution separation of peptide mixtures by reversed-phase high-performance liquid chromatography, J. Chromatogr. A. 296 (1984) 31–59.

[23] U.D. Neue, Theory of peak capacity in gradient elution, J. Chromatogr. A. 1079 (2005) 153–161.

[24] L.R. Snyder, J.W. Dolan, J.R. Gant, Gradient elution in high-performance liquid chromatography, J. Chromatogr. A. 165 (1979) 3–30.

[25] V.L. McGuffin, C.E. Evans, S.H. Chen, Direct examination of separation processes in liquid chromatography: Effect of temperature and pressure on solute retention, J. Microcolumn Sep. 5 (1993) 3–10.

[26] V.L. McGuffin, S.-H. Chen, Molar enthalpy and molar volume of methylene and benzene homologues in reversed-phase liquid chromatography, J. Chromatogr. A. 762 (1997) 35–46.

[27] M. Martin, G. Guiochon, Effects of high pressure in liquid chromatography, J. Chromatogr. A. 1090 (2005) 16–38.

[28] D. V. McCalley, The impact of pressure and frictional heating on retention, selectivity and efficiency in ultra-high-pressure liquid chromatography, TrAC - Trends Anal. Chem. 63 (2014) 31–43.

[29] M.M. Fallas, U.D. Neue, M.R. Hadley, D. V. McCalley, Further investigations of the effect of pressure on retention in ultra-high-pressure liquid chromatography, J. Chromatogr. A. 1217 (2010) 276–284.

[30] M.M. Fallas, N. Tanaka, S.M.C. Buckenmaier, D. V. McCalley, Influence of phase type and solute structure on changes in retention with pressure in reversed-phase high performance liquid chromatography, J. Chromatogr. A. 1297 (2013) 37–45.

[31] M.M. Fallas, U.D. Neue, M.R. Hadley, D. V. McCalley, Investigation of the effect of pressure on retention of small molecules using reversed-phase ultra-high-pressure liquid chromatography, J. Chromatogr. A. 1209 (2008) 195–205.

[32] M.M. Fallas, M.R. Hadley, D. V. McCalley, Practical assessment of frictional heating effects and thermostat design on the performance of conventional (3 μm and 5 μm) columns in reversed-phase high-performance liquid chromatography, J. Chromatogr. A.

1216 (2009) 3961–3969.

[33] D. Åsberg, J. Samuelsson, M. Leśko, A. Cavazzini, K. Kaczmarski, T. Fornstedt, Method transfer from high-pressure liquid chromatography to ultra-high-pressure liquid chromatography: II: Temperature and pressure effects, J. Chromatogr. A. 1401 (2015) 52–59.

[34] V.L. McGuffin, C.E. Evans, Influence of pressure on solute retention in liquid chromatography, J. Microcolumn Sep. 3 (1991) 513–520.

[35] S. Fekete, J.L. Veuthey, D. V. McCalley, D. Guillarme, The effect of pressure and mobile phase velocity on the retention properties of small analytes and large biomolecules in ultra-high pressure liquid chromatography, J. Chromatogr. A. 1270 (2012) 127–138.

Table I. Overview of system configurations assessed during performance characterization study.

Configuration	Pre-column tubing i.d. (µm) × length (mm)	Post-column tubing i.d. (µm) × length (mm)	Flow-cell volume (µL)	Extra-column variances (μl^2)
#1	75×350	75×350	0.045	0.99
#2	100×350	75×350	0.045	1.24
#3	75×350	75×350	2.5	3.67
#4	100×350	75×350	2.5	4.64
#5	75×350	100×350	2.5	4.62
#6	100×350	100×350	2.5	5.81

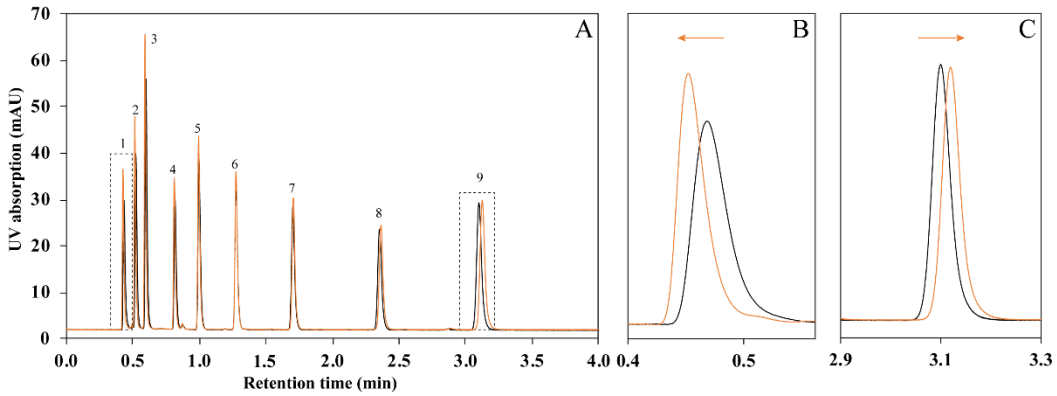

F

Figure 1. Effect of tubing configuration (75 µm – orange trace *vs.* 100 µm i.d. – black trace) on resulting separation performance measured in isocratic mode at optimal mobile-phase velocity. (B) and (C) shows the zoom-in panels for uracil and benzanthracene, respectively. Experimental conditions: mobile-phase composition: F = 0.4 mL/min; 70:30% (v/v) ACN:H_2O; column-oven configuration: still-air mode at 35°C; and using a 2.5 µL flow cell. Peak identification: (1) uracil, (2) phenol, (3) acetophenone, (4) butyrophenone, (5) valerophenone, (6) hexanophenone, (7) heptanophenone, (8) octanophenone, and (9) benzanthracene.

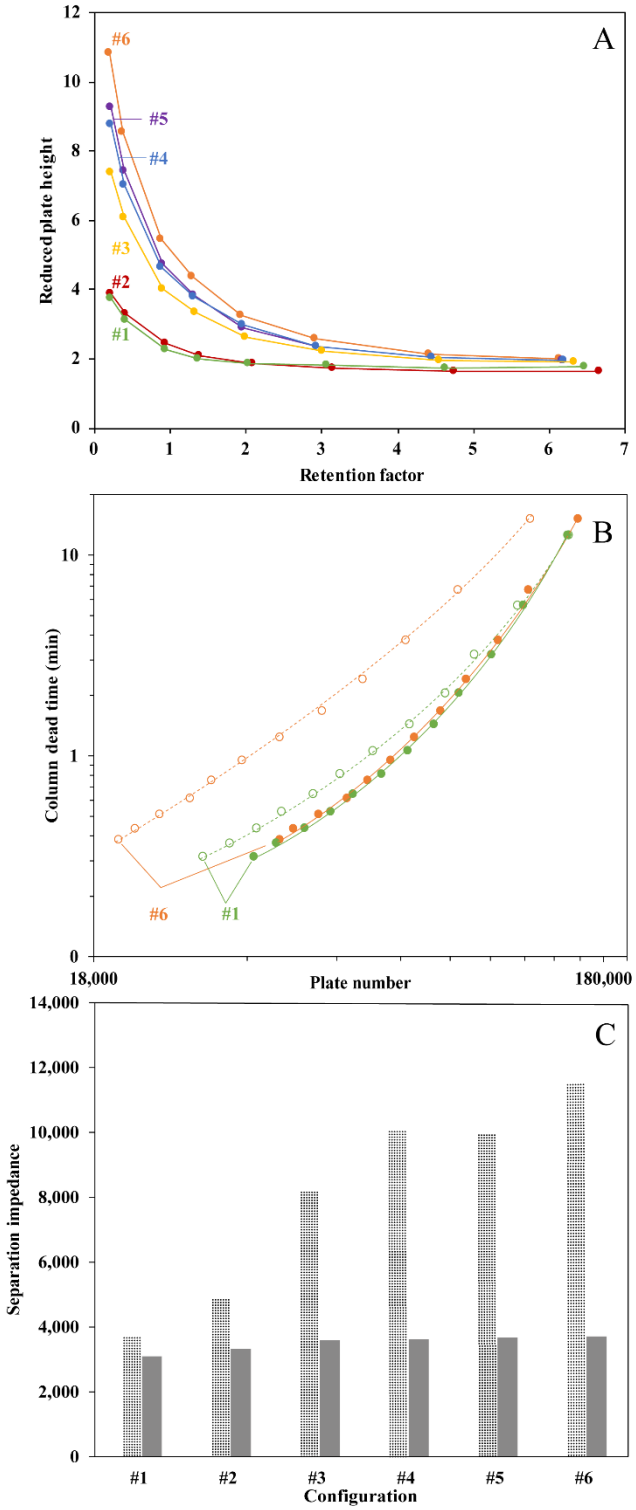

Figure 2. Quantitative assessment of tubing and flow-cell configuration as function of retention factor. (A) Effect on chromatographic dispersion, (B) effect on kinetic performance limits at ΔP = 1500 bar (early-eluting analyte (k = 0.95) marked with solid line, late-eluting analyte (k = 6.1) marked with dotted line), and (C) effect on separation impedance for k = 0.95 marked

with dotted area, and k = 6.1 marked with solid area. Information on system configurations is provided in Table I.

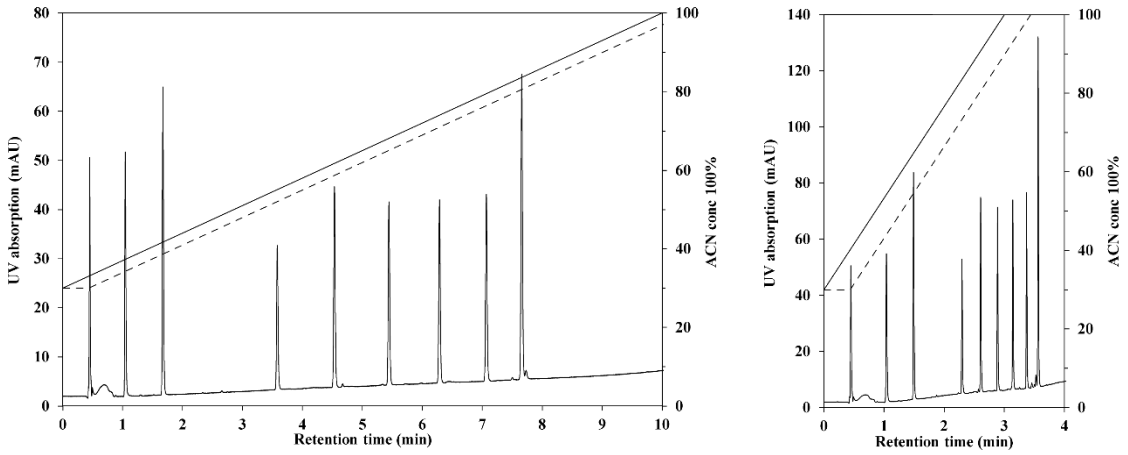

Figure 3. Chromatograms obtained with configuration #1 by applying a 10 min conventional gradient (A) and a steep 3 min gradient (B). Experimental conditions: F = 0.4 mL/min; secondary y-axis depicts the aqueous ACN gradient (programmed and actual gradient profile are displayed by solid and dashed lines, respectively); column-oven configuration: still-air mode at 35°C. Peak identification is similar as in Fig. 1.

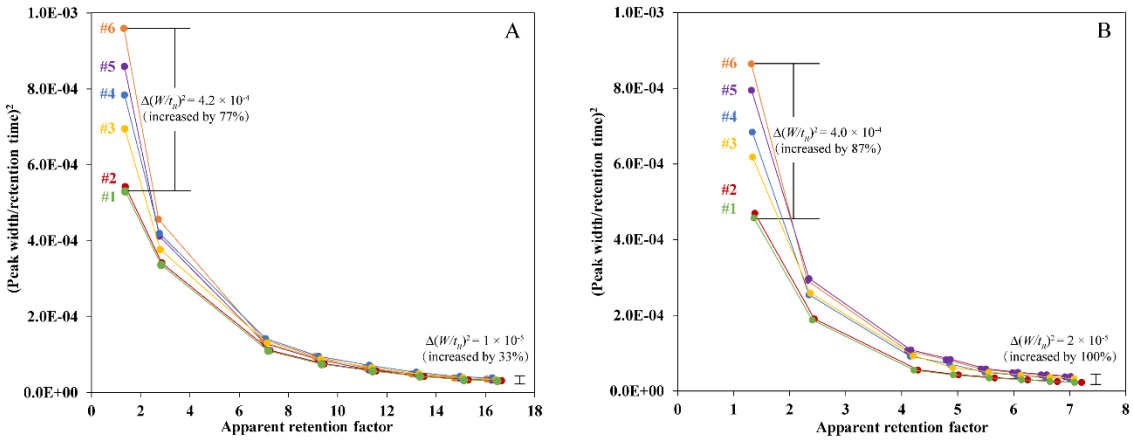

Figure 4. Plot of the square of the peak width normalized by retention time as function of apparent retention factor for different instrument configurations, see Table I, recorded in gradient mode applying a gradient duration of 10 min (A) and 3 min (B), respectively.

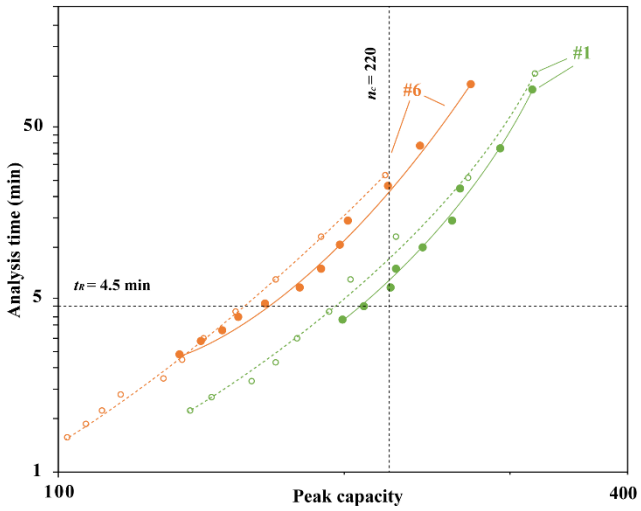

Figure 5. Effect of tubing and flow-cell configuration on kinetic performance limits recorded in gradient mode applying steep gradients with t_G/t_0 = 7 at ΔP = 1500 bar. Early-eluting analyte (k^* = 1.3) are marked with solid line, late-eluting analyte (k^* = 7.2) are marked with dotted line.

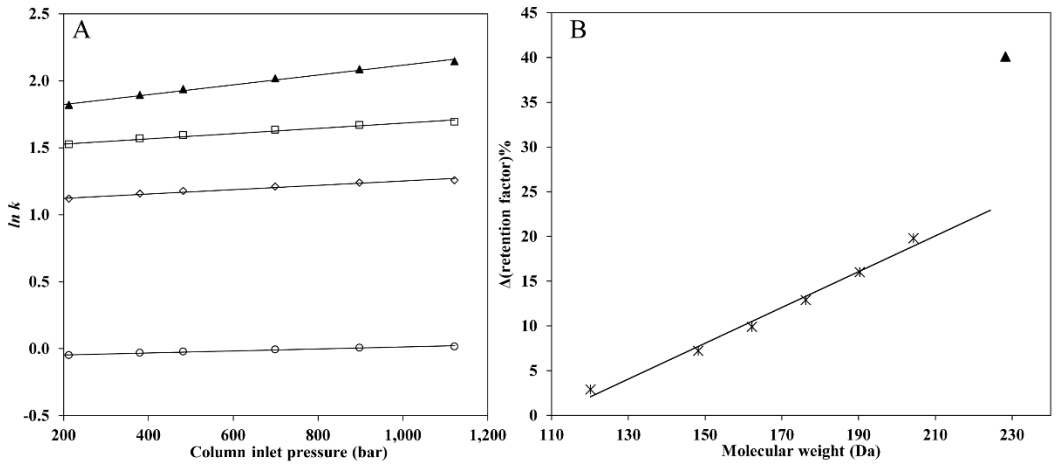

Figure 6. (A) The natural logarithm of retention factor (*ln k*) as a function of the column inlet pressure recorded for butyrophenone (open circles), heptanophenone (open diamonds), octanophenone (open squares), benzanthracene (solid triangles) when adding restrictors behind the UV flow cell. (B) Shows the effect of molecular weight on retention factor change in percentage for alkylphenones and benzanthracene. Experimental conditions: flow rate F = 0.1 mL/min; mobile-phase composition: 70:30% (v/v) ACN:H_2O; column-oven configuration: still-air mode at 35°C.

Supplementary Material

Assessing effects of UHPLC instrument configuration on dispersion, system pressure, and retention

Zhuoheng Zhou[1], Mauro De Pra[2], Frank Steiner[2], Gert Desmet[1], Sebastiaan Eeltink[1,*]

[1]Vrije Universiteit Brussel (VUB), Department of Chemical Engineering, Brussels, Belgium

[2]Thermo Fisher Scientific, Germering, Germany

(*) corresponding author

Pleinlaan 2, B-1050, Brussels, Belgium

Tel.: +32 (0)2 629 3324, Fax: +32 (0)2 629 3248, E-mail: seeltink@vub.be

Table of contents

SM-1. Effect of system configuration on system residence time.

SM-2. Effect of pre- and post-column tubing on dispersion in presence and absence of sample focusing.

SM-3. Establishing kinetic performance limits in gradient mode.

SM-1. Effect of system configuration on system residence time

The system residence time ($t_{0,sys}$) is assumed to be the sum of individual residence time contributions of individual components in the flow path:

$$t_{0,sys} = t_{inj} + t_{pre-tub} + t_{post-tub} + t_{0,column} + t_{flow-cell} \quad \text{(S2)}$$

For incompressible fluids, the flow rate remains constant throughout the flow path, and Eq. S2 can be rewritten as:

$$t_{0,sys} = \frac{V_{inj}+V_{pre-tub}+V_{post-tub}+V_{0,column}+V_{flow-cell}}{F} \quad \text{(S3)}$$

where V is the fluidic volume of different components. Thus the difference in system residence time ($\Delta t_{0,sys}$) between different configurations can be determined as

$$\Delta t_{0,sys} = \frac{\Delta V_c}{F} \quad \text{(S4)}$$

where ΔV_c change in volume altering configuration. The volumes of different flow-path components were calculated and are summarized in Table S1.

Table S1. Fluidic volumes and pressure drop on different flow-path components measured at u_{opt} and 35°C applying a mobile-phase composition of 70:30% (v/v) ACN:H_2O.

Components	Nominal volume (µL)	ΔP (bar) at F = 0.4 mL/min
Injector (after needle seat)	< 0.225 µL	8
75 µm × 350 mm tubing	1.55	18
100 µm ×350 mm tubing	2.75	4

45 nL flow cell	1.6*	68**
2.5 µL flow cell	2.5	3
2.1 mm i.d. × 100 mm column	161.6***	663

* 75 µm i.d. × 350 mm pre-column tubing volume included.

** 75 µm i.d. × 350 mm pre-column and post-column tubing included.

*** Based on t_0 measurements.

When comparing configurations #3 and #6, the i.d. of pre-and post-column tubing increases from 75 µm to 100 µm while other component remain the same, which leads to an increase in volume from 3.1 µL (2 ×1.55 µL) to 5.5 µL (2 ×2 .75 µL). Using Eq. S4, the increase in residence time is determined to be 0.006 min. In isocratic experiment, $t_{0,sys}$ of #3 and #6, measured as the retention time of uracil, were determined to be 0.426 min and 0.434 min, respectively (separation conditions see *'Section 2.2'* in the main manuscript). The observed residence time difference is thus 0.008 min, which matches well with the predicted value based on Eq. S4.

SM-2. Effect of pre- and post-column tubing on dispersion in presence and absence of sample focusing

Fig. S1 show the effect of i.d. of pre- and post-column tubing on dispersion characteristics (comparing configurations #4 and #5) measured in isocratic mode in the presence and absence of a sample-focusing effect. Fig. S1A show the reduced plate height as function of retention factor in the absence of an focusing effect, where the mobile phase composition (70:30% (v/v) ACN:H_2O) matches that of the sample. Fig. S1B shows the dispersion when increasing the water content in the sample mixture, *i.e.*, using 50:50% (v/v) ACN:H_2O.

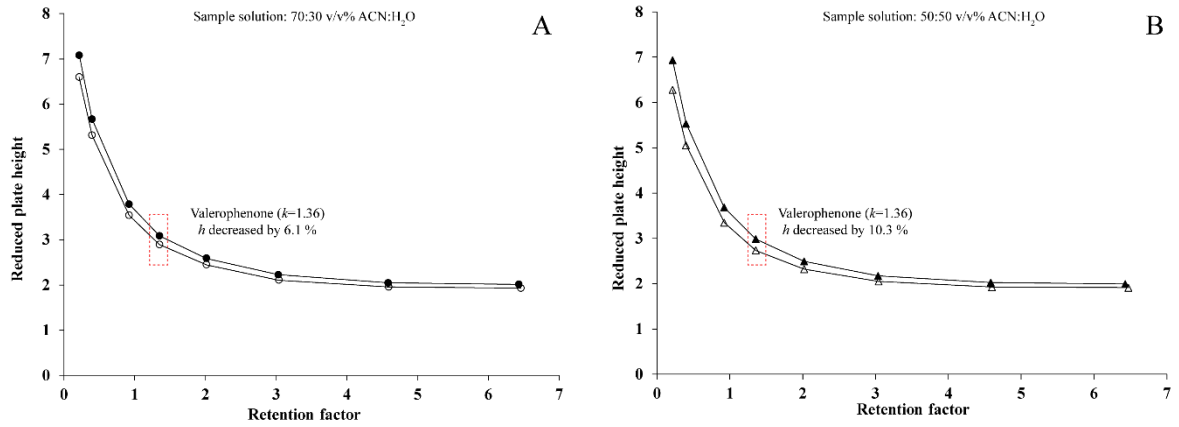

Figure S1. Comparison of separation efficiency between configuration #4 (open symbols) and #5 (solid symbols) applying different sample solution conditions: (A) sample dissolved in 70:30% (v/v) ACN:H_2O and (B) in 50:50% (v/v) ACN:H_2O. Valerophenone (k=1.36, marked with dotted red box) was selected as an indicator to highlight the difference in dispersion.

When the sample dissolved in solution containing higher water content, the sample band is focused on the column head, and pre-column dispersion is less detrimental. As a result, the configuration with smaller post-tubing i.d. (configuration #4) results in slightly better performance.

SM-3. Establishing kinetic performance limits in gradient mode.

Experimental peak capacities (n_c) were determined based on the gradient duration and the $4\sigma_t$ peak width. The kinetic limit of peak variance ($\sigma_{t,KPL}$) and analysis time ($t_{R,KPL}$) at maximum operating pressure (ΔP_{max}) can be expressed as [1]:

$$\sigma_{t,KPL} = \sqrt{\frac{\Delta P_{max} \cdot K_V \cdot H}{u_0 \cdot \eta}} \cdot \frac{(1+k_e)}{u_0} \quad \text{(S5)}$$

$$t_{R,KPL} = \frac{\Delta P_{max} \cdot K_V}{u_0^2 \cdot \eta} \cdot (1 + k^*) \quad \text{(S6)}$$

where k_e the gradient retention factor during elution and k^* is the apparent gradient retention factor that is calculated based on the t_R and t_0 time.

According to linear solvent strength model (LSS), with a defined gradient steepness (b) expressed as:

$$b = S \cdot \Delta\phi \cdot \frac{t_0}{t_G} \quad \text{(S7)}$$

a simplified expressions of k_e and k^* can be written as [2,3]:

$$k_e = \frac{1}{b} \tag{S8}$$

$$k^* = \frac{1}{b} \cdot ln(b \cdot k_0 + 1) \tag{S9}$$

where S is the slope of the linear relationship between ln k and organic solvent concentration, $\Delta\phi$ is the mobile-phase composition range and k_0 is the retention factor at the start of gradient. Substituting parameters in Eqs. 9 and 11 by combining Eqs. 10, 12 and 13 results in the governing equation set for obtaining the kinetic performance limits in gradient mode:

$$n_{c,KPL} = 1 + \frac{1}{4} \cdot \sqrt{\frac{\Delta P_{max} \cdot K_V}{u_0 \cdot \eta \cdot H}} \cdot \frac{S \cdot \Delta\phi}{S \cdot \Delta\phi \cdot \frac{t_0}{t_G} + 1} \tag{S10}$$

$$t_{R,KPL} = \frac{\Delta P_{max} \cdot K_V}{u_0^2 \cdot \eta} \cdot \left[1 + \frac{t_G}{t_0} \cdot \frac{1}{S \cdot \Delta\phi} \cdot ln\left(\frac{t_G}{t_0} \cdot \frac{k_0}{S \cdot \Delta\phi} + 1\right)\right] \tag{S11}$$

The fixed-length kinetic plot data can be extrapolated when operating at the maximum system pressure while maintaining t_G/t_0:

$$n_{c,KPL} = 1 + \sqrt{\lambda} \cdot \left(n_{c,exp} - 1\right) \tag{S12}$$

$$t_{R,KPL} = \lambda \cdot t_{R,exp} \tag{S13}$$

where λ can be considered as column length rescaling factor, given by:

$$\lambda = \frac{\Delta P_{max}}{\Delta P_{exp}} \tag{S14}$$

References

[1] K. Broeckhoven, D. Cabooter, F. Lynen, P. Sandra, G. Desmet, The kinetic plot method applied to gradient chromatography: Theoretical framework and experimental validation, J. Chromatogr. A. 1217 (2010) 2787–2795.

[2] U.D. Neue, Theory of peak capacity in gradient elution, J. Chromatogr. A. 1079 (2005) 153–161.

[3] U.D. Neue, J.R. Mazzeo, A theoretical study of the optimization of gradients at elevated temperature, J. Sep. Sci. 24 (2001) 921–929.